Nanoscale

PAPER

View Article Online
View Journal | View Issue

Cite this: *Nanoscale*, 2023, **15**, 171

Humidity sensors based on molecular rectifiers†

Ryan P. Sullivan, [a] Eduardo Castellanos-Trejo,[a] Renate Ma,[b] Mark E. Welker [b] and Oana D. Jurchescu *[a]

Received 16th August 2022,
Accepted 2nd December 2022

DOI: 10.1039/d2nr04498f

rsc.li/nanoscale

Ambient humidity plays a key role in the health and well-being of us and our surroundings, making it necessary to carefully monitor and control it. To achieve this goal, several types of instruments based on various materials and operating principles have been developed. Reducing the production costs for such systems without affecting their sensitivity and reliability would allow for broader use and greater efficiency. Organic materials are prime candidates for incorporation in humidity sensors given their extraordinary chemical diversity, low cost, and ease of processing. Here, we designed, assembled and tested humidity sensors based on molecular rectifiers that can electrically transduce the changes in the ambient humidity to offer accurate quantitative information in the range of 0 to 70% relative humidity. Their operation relies on the changes occurring in the electric field experienced by the molecular layer upon absorption of the polar water molecules, resulting in modifications in the height and shape of the tunneling barrier. The response is reversible and reproducible upon multiple cycles and, coupled with the simplicity of the device architecture and manufacturing, makes these nanoscale sensors attractive for incorporation in various applications.

Introduction

Ambient humidity can vary greatly depending on the geographical location, the season and even the time of day. Monitoring and controlling it is of utmost importance since it affects the corrosion in buildings, vehicles and infrastructure, the operation of industrial equipment, and the quality of the products and goods.[1,2] Our well-being is also very much dependent on the ambient humidity since both our health and comfort are optimal in a narrow humidity window. Uncontrolled environmental moisture can lead to a reduction in shelf life and performance degradation in electronic devices playing key roles in energy, communication, security, or medical fields.[3–5] Given its profound impact on multiple sectors of our lives, the development of sensors for monitoring environmental humidity is an active area of research. Various types of equipment that can monitor humidity in both industrial and household settings have been proposed. These instruments operate on different principles and incorporate a wide range of materials from electrolytes to porous ceramics, polymers, or composites thereof.[6,7] Commercially available humidity-sensing technologies are diverse, ranging from units relying on monitoring capacitive, resistive, or thermal conductance changes occurring in material properties upon interaction with water vapor, to exploiting acoustic, optical or electromechanical effects.[6,8–10] The versatility in chemical structure offered by organic compounds allows for synthetic designs that target specific interactions with water, and hence they quickly became popular in the humidity sensing arena, alongside active components in chemical and biological sensors.[11–17] Single-molecule-based sensors are particularly attractive since they can be integrated into semiconductor array chips to provide the much-sought electronics miniaturization. Additionally, they are manufactured by low-cost, high-throughput techniques and hence can be easily mass-produced and deployed. One such molecular-scale device is the molecular rectifier (diode), which was shown to efficiently transduce the ambient moisture absorbed in a monolayer to an electrical signal under special conditions.[18] Analogous to the conventional diodes, the molecular rectifiers induce an asymmetry between the current measured under forward and reverse bias regimes, with the figure of merit being the rectification ratio $R = |J(+V)/J(-V)|$, where J is current density at the applied voltage V. Toggling between low and high humidity environments resulted in a reversible and consistent change in R,[18] but so far, to the best of our knowledge, no quantitative dependence of R *versus* relative humidity (RH) has been reported. These demonstrations represent important milestones since they offered proof of concept that humidity sensing is possible in molecular diodes, but the development of systems that can allow the generation of a calibration curve with intermediate RH values is necessary to

[a]*Department of Physics, Center for Functional Materials, Wake Forest University, Winston-Salem, NC, 27109, USA. E-mail: jurchescu@wfu.edu*
[b]*Department of Chemistry, Center for Functional Materials, Wake Forest University, Winston-Salem, NC, 27109, USA*

† Electronic supplementary information (ESI) available. See DOI: https://doi.org/10.1039/d2nr04498f

be able to accurately monitor and control the ambient humidity using molecular diodes.

In this work, we designed, fabricated, and tested a nanoscale humidity sensor based on a molecular rectifier that can provide accurate quantitative information on RH in the range of 0–70%. The molecular monolayer consists of a self-assembled monolayer (SAM) and the water detection mechanism relies on altering the dipolar field within the device upon absorption of water molecules. The sensor operates at low voltages (max 2 *V*), and subtle changes in ambient humidity give rise to clear and reproducible changes in *R*. The response is fully reversible upon multiple RH cycles and the simple electrode/monolayer/electrode structure could enable low-cost production and facile integration with other circuitry elements to develop advanced applications.

Results and discussion

The molecular rectifier–based humidity sensor consists of an (*E*)-1-([2,2′-bithiophen]-5-yl)-*N*-(3-(triethoxysilyl)propyl)methanimine (BT-TESP-MA) SAM sandwiched between a bottom electrode consisting of a highly doped silicon substrate with a thin naturally forming SiO_2 layer on its surface, and an eutectic gallium indium (EGaIn) top electrode. The soft nature of the top electrode ensures a high yield (>90%) in the measurements since it preserves the quality of the SAM layer and can be efficiently used even below its freezing temperature (16 °C), as proven by the successful testing of SAMs at temperatures as low as −160 °C.[19,20] The SAM was deposited at the surface of the silicon oxide layer from a solution in chloroform following the procedures described in the Experimental section. The triethoxysilyl head of the molecule bonds to the SiO_2 layer *via* covalent Si–O bonds to spontaneously form a monolayer, while the bithiophene tail group is a humidity-sensitive functional moiety that facilitates interactions with water molecules. Details on the synthesis and chemical characterization of the SAM are provided in the Experimental section and ESI.† The devices were characterized in a bespoke vacuum-sealed chamber that was either purged with dry (channel 1 in Fig. 1) or water-saturated air (channel 2 in Fig. 1), while the RH was constantly monitored with a NIST-traceable psychrometer. All tests were performed at room temperature. The schematic configuration of the testing setup, as well as the structure of the SAM and the molecular rectifier, are included in Fig. 1. The porous and rough nature of the surface of the Ga_2O_3 oxide layer that naturally forms on the surface of the EGaIn contact (Fig. 2a) results in an effective contact area of $\sim 10^{-4}$ of the geometrical area, allowing water molecules introduced in the measurement chamber to come into contact with the SAM without disturbing the molecular junction.[21–23] The SAM rectifies the current, with an $R = 33 \pm 3$ in dry air (see the black curve in Fig. 2b, where the logarithm of the absolute current density is plotted *versus* voltage). This rectification strength is lower than that obtained in other SAM-based rectifiers since these molecules have not been specifically designed and/or optimized for efficient current rectification.[20,24–32] What is important, however, is that humidity has a notable effect on the current–voltage (*I*–*V*) characteristics of these molecular diodes, as can be seen in Fig. 2b: the reverse current is reduced by a factor of 5, whereas the forward current increases by about 50% in the samples measured under 70% RH (red curve), compared to the benchmark obtained in dry air, yielding a rectification ratio of $R = 160 \pm 10$. Since bare SiO_2 is hygroscopic, we also tested if water surface condensation has

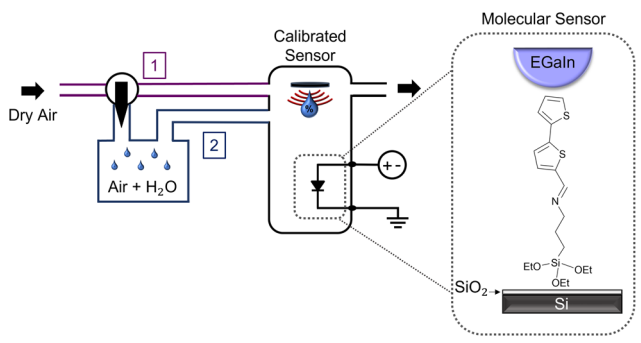

Fig. 1 Configuration of the setup used for testing molecular diodes as humidity sensors. The delivery and control of the water vapours is shown on the left and the device structure on the right.

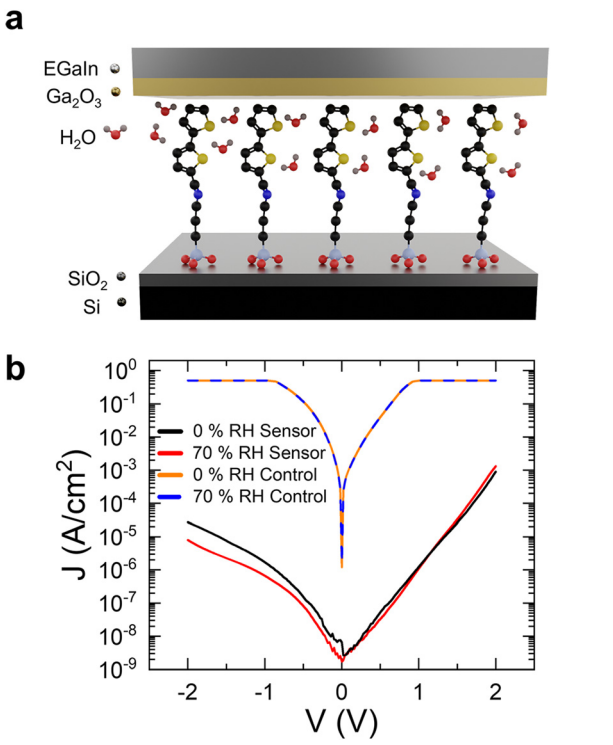

Fig. 2 (a) Molecular rectifier device structure with BT-TESP-MA SAM molecules sandwiched between the Si/SiO_2 and EGaIn electrodes interacting with water molecules. (b) The current density *versus* voltage curves for the molecular humidity sensor based on the BT-TESP-MA monolayer for low and high humidity. The substrate response (control) is included for reference.

an effect on the electrical properties of our substrates and found that there is a negligible difference between the measurements taken under 70% RH (blue) or dry air (orange) in the absence of the SAM, confirming that the interactions between BT-TESP-MA and the water molecules are solely responsible for the changes in the electrical response of our molecular rectifiers.[23] While these instabilities are unwanted in conventional circuits because they render them unreliable and unpredictable, they can be harnessed to detect the RH value if the response is reproducible and reversible. To benchmark the changes in electrical properties upon exposure to water vapours, the rectification ratios of the molecular diodes were measured as a function of the relative humidity (Fig. 3a, black). We found that R depends linearly on RH (Pearson's r = 0.99) from 0 to 70% RH, with an adjusted R^2 of 0.98, following the expression $R/R_0 = 5.2 \cdot \mathrm{RH} + 0.91$. Here the results have been normalized with respect to the rectification ratio value obtained in dry air. The properties were reproducible upon repeated cycles of ascending RH (red points in Fig. 3a) and have been completely restored upon cycling the humidity in the reverse direction (blue points). The bare Si/SiO_2 substrates with the EGaIn top contact showed no rectifying behaviour and the changes recorded in the same RH range were significantly inferior to those exhibited by the SAM, and thus can be ignored (grey points in Fig. 3a). This observation is important since it also confirms that water electrolysis, if occurring, does not contribute significantly to the effects observed here and hence can be ignored in elucidating the mechanism for humidity sensing. The reversibility of the response is also illustrated in Fig. 3b, where the samples were cycled between high (70%) and low RH (labelled 0%) several times, resulting in a consistent switching in R (black) and negligible switching due to the substrate alone (light grey). For reference, we also include the response of a SAM that consists of alkyl chains, with no other functional groups, namely triethoxy(octyl)silane (burgundy). The changes in R for this molecule are extremely small ($R/R_0 < 2$, with $R_0 = 4.19 \pm 0.05$), suggesting that the presence of the thiophene end-group is critical in the sensing mechanism, as we will discuss later. When cycling between 0 and 70% RH, the total rise time was determined to be approximately 10 min with a fall time of 35 min as shown in Fig. S1.†

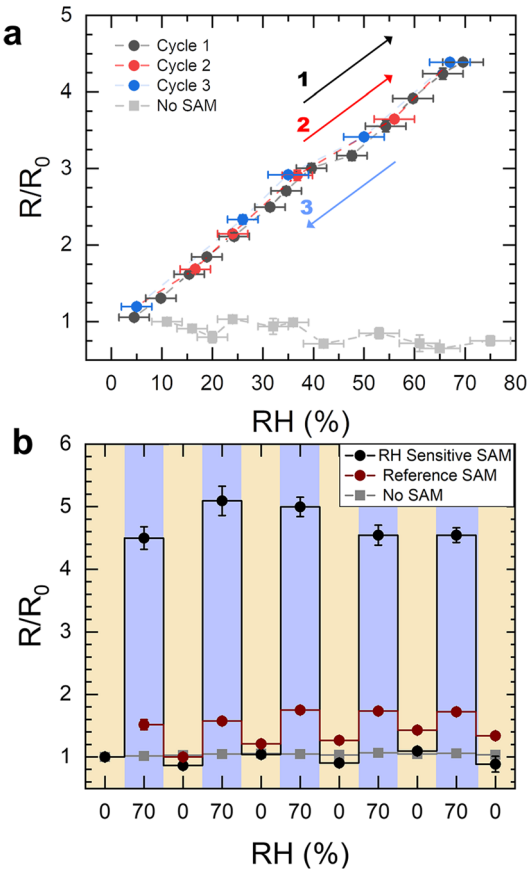

Fig. 3 (a) Dependence of the normalized R on RH for two ascending cycles (1 and 2) and one descending cycle (3) upon a 5 min exposure time for each point. The x-axis error is dominated by the accuracy of the calibrated sensor, but it also considers any RH deviations measured inside the chamber during the 10 min exposure. (b) The normalized R when cycling between low and high RH using a rise time of 10 min and fall time of 30 min. The y-axis error represents the standard deviation of repeated measurements.

The mechanisms through which polar molecules, including water, can be sensed by organic semiconductors (OSCs) have been extensively discussed throughout the literature.[14,33,34] For organic thin-film transistors not dominated by contact effects, for example, dipole-induced charge trapping at grain boundaries represents the major effect, while in short-channel length devices, where the contacts become more relevant, the interactions between analytes and the contacts dominate the response.[35] In these latter devices, injected charge carriers accumulate close to the organic semiconductor/electrode interface and induce an image charge in the metal electrode, which results in the formation of interface dipoles. Upon absorption, polar analytes alter (shield or enhance) the net interface dipole, thus adjusting the Schottky barrier which, in turn, directly affects charge injection.[36–38] The formation of the interface dipoles was investigated by measuring the change in the ionization potential. For example, the chemisorption of NO_2 was found to induce a change in film ionization potential up to 650 mV resulting from the band bending due to the dipolar field it introduces.[33] To elucidate if a similar phenomenon occurs in our molecular diodes in the presence of water molecules, we measured the shifts in the work function of a silicon substrate treated with BT-TESP-MA SAM *versus* RH utilizing the Kelvin probe technique.[39,40] The instrument was placed inside the same chamber setup illustrated in Fig. 1 that was used for the electrical characterization of the rectifiers. At RH = 0% the BT-TESP-MA/SiO_2 work function shifted by $\Delta\Phi = -0.43 \pm 0.03$ eV with respect to the untreated substrate due to the internal dipole of the SAM molecule (μ_{SAM}), which modifies the surface potential. The magnitude and direction of the shift are dictated by the strength of the SAM intrinsic dipole and its orientation with respect to the surface, with the SAM density playing a crucial role.[41–43] Remarkably, the work function of the SAM-modified silicon changed by roughly $\Delta\Phi$ =

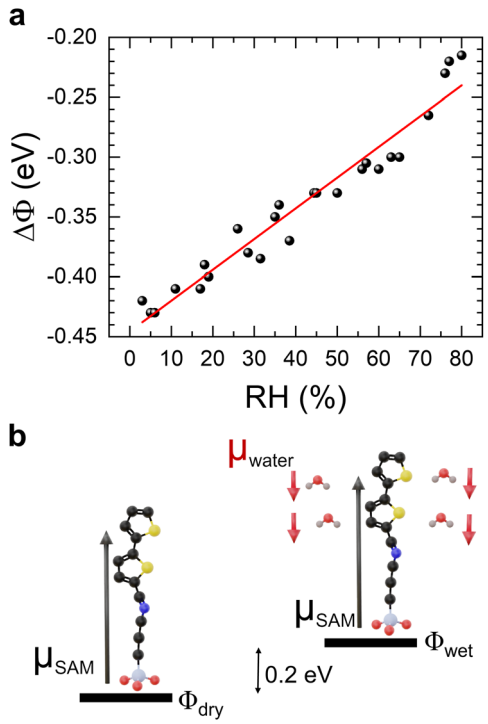

Fig. 4 (a) Work function shift of SAM-modified Si/SiO_2 substrate as a function of the surrounding RH. (b) Schematic of the effects contributing to the work function shift of the SAM-modified silicon due to the shielding effects from the dipoles of the water molecules.

200 mV when adjusting the RH from 0 to 70% (Fig. 4a) and depended linearly on the relative humidity, similar to the rectification ratio (Fig. 3a). In contrast, the work function of the silicon substrate exhibited a negligible change ($\Delta\Phi \approx 10$ mV) over the same range. This finding suggests that the adsorption of water molecules in our devices induces additional interface dipoles around the contact-SAM interface due to the internal dipole moment of the water molecule ($\mu_{water} = 1.86$ D).[44] While a detailed description of the mechanism responsible for water sensing will not be attempted given the multiple processes that could play a role, as well as possible interferences with other species present in the atmosphere, which make it extremely complex, in Fig. 4b we sketch the phenomena that could lead to the measured shift in the net dipole moment in the rectifier. Water molecules that penetrate the molecular rectifier are likely to interact with the SAM molecules *via* noncovalent bonds (hydrogen bonds or π interactions), disrupting intermolecular interactions within the monolayer and inducing local fields that are superimposed on the applied voltage. As a result, the net field experienced by the molecule changes monotonically upon gradual absorption of the water molecules, altering the height and shape of the tunneling barrier and consequently the current magnitude. This effect results in a steady change in R, similar to the case when the internal dipole moment determined strictly by the molecular structure of the SAM enhanced the rectification strength of the molecular rectifiers.[25,29] The formation of a thiophene-water complex is also possible, which has been shown to be stabilized by C–H···O, O–H···S, and O–H···π interactions.[45] Indeed, other SAMs containing a thiophene rather than bithiophene functional group in their structure responded to water vapours in a similar manner (Fig. S2†). Nevertheless, the stability across multiple cycles was reduced in this case, a subject that is under study. To evaluate whether the molecular interactions involving the imine bond present in our molecules contribute to the observed device response, we further tested molecular diodes based on (*E*)-1-phenyl-*N*-(3-(triethoxysilyl)propyl)methanimine, a molecule containing the imine bond, but not the thiophene functional group; results are shown in Fig. S3.† It can be observed that the rectification ratio is independent of the relative humidity in this case, suggesting that the interaction with the imine does not contribute to the humidity sensing mechanism.

Experimental

Device fabrication

We fabricated the molecular rectifiers on highly n-doped silicon wafers (resistivity of 0.001–0.005 Ω cm) with a thin native oxide layer (≈ 2 nm) that were cut into 1 × 1 cm substrates. The wafers were cleaned by a 10-minute acetone bath at 85 °C; rinsed with acetone, followed by isopropyl alcohol (IPA); a 10 min IPA bath at 85 °C; rinsed with IPA then blown dry with nitrogen; exposed to UV ozone for 10 min; then thoroughly rinsed with deionized water and blown dry with nitrogen. Self-assembly of the molecular monolayers occurred inside a nitrogen glovebox (<0.1 ppm H_2O, <0.1 ppm O_2), where the substrates were submerged using a glass jar containing 7 mM solution of the SAM in room-temperature chloroform for 16–24 hours. Afterwards, the substrates were thoroughly rinsed with chloroform, then IPA, and were blown dry with nitrogen. The electrical characterization was performed immediately after fabrication.

Electrical characterization

Devices were characterized in a custom-made vacuum-sealed chamber that was either purged with dry air or water-saturated air as illustrated in Fig. 1. The RH of the camber was constantly monitored using an Extech RH300 NIST-traceable psychrometer (accuracy ± 3%). The samples were maintained for a minimum of 5 min at a given RH, which is a significantly larger time interval than the time needed to adjust the RH inside the chamber and for the calibrated sensor to respond. The SAMs were electrically characterized in a metal/SAM/metal sandwich configuration. A malleable top contact was formed by dipping a 0.5 mm tungsten tip into eutectic gallium indium (EGaIn). The geometrical area of the EGaIn area was estimated to be 0.020 ± 0.006 mm^2. A rough Ga_2O_3 layer forms on the surface of the EGaIn electrode allowing targeted analytes to directly interact with the underlying SAM.[22] An external potential was applied to the top EGaIn electrode, while the silicon substrates, acting as bottom contacts, were grounded. The

molecular junctions were measured using an Agilent 4155C semiconductor parameter analyser. The rectification ratio, R, was calculated as the ratio between the current density J at a forward bias ($+V$) and the current density at a reverse bias ($-V$). The current density was obtained by dividing the measured current by the geometrical area of the EGaIn probe tip. The rectification ratios for all SAMs were calculated at ± 2 V, while for the untreated substrates we used ± 1 V as the current values reached the compliance of our instrument at higher voltages.

Work function determination

The shift in the work function of the Si/SiO_2 substrate upon self-assembly of BT-TESP-MA and as a function of RH were analysed using a Trek model 325 electrostatic voltmeter configured for Kelvin probe measurements. The Kelvin probe was calibrated using highly-ordered pyrolytic graphite (HOPG) and placed in the same environmental chamber that was used for characterising the molecular rectifiers. The work function Φ, of the untreated substrate, as well as of the treated substrate was determined by the expression:

$$\Phi = -e(V_{SAM} - V_{HOPG}) + \Phi_{HOPG} \quad (1)$$

where e is the elementary charge, V_{SAM} is the signal measured on the blank or SAM-modified Si substrate, V_{HOPG} is the signal from HOPG and Φ_{HOPG} is the work function of HOPG (Φ_{HOPG} = 4.48 eV).[40] Clean untreated substrates in dry air were used as a reference for all the work function data. Negligible changes in the measured work function of HOPG were found for the same ranges of RH.

BT-TESP-MA synthesis

The aromatic-*N*-(3-(triethoxysilyl)propyl)methanimines used in this study were gathered from the reactions of the appropriate benzaldehydes with (3-aminopropyl)triethoxysilane as described previously with more details in the ESI†.[28,46] All methanimines used in this work were analysed by ^{13}C and ^{1}H nuclear magnetic resonance spectroscopy (NMR) and high-resolution mass spectrometry (HRMS) which are included in the ESI (Fig. S4–S9).†

Conclusions

In summary, we developed nanoscale humidity sensors based on molecular diodes consisting of SAMs sandwiched between silicon substrates and a EGaIn contact. The detection relies on the consistent and reproducible changes observed in the current–voltage characteristics of these diodes upon interaction with water vapor: the current rectification exhibits a linear dependence on the relative humidity for ranges of 0–70%, with a maximum relative change in the rectification ratio of 5 recorded for high humidity environments. The changes are completely reversible upon multiple cycles and result from the modifications in the interface dipole environment upon the absorption of the polar water molecule, confirmed by the 0.2 eV shift measured in the work function, which alter the height and shape of the tunneling barrier. Our results highlight a novel practical application for molecular rectifiers as highly sensitive humidity sensors. Further tuning of the molecular structure could allow the detection of other analytes in the future which, coupled with the low fabrication cost and integrability with current silicon technologies, could lead to new paradigms for sensing technologies.

Author contributions

R. P. S, M. E. W. and O. D. J conceptualized the project and designed the experiments. R. M. synthesized the SAMs and executed the chemical characterization of the new compounds under the supervision of M. E. W. R. P. S. and E. C.-T. fabricated the samples, performed the electrical characterization, and analysed the data under the supervision of O. D. J. R. P. S. and O. D. J. wrote the manuscript. All authors contributed to the discussions and edited the manuscript.

Conflicts of interest

There are no conflicts to declare.

Acknowledgements

This work was partially supported by the National Science Foundation through Grants No. ECCS-1810273 and CMMI-2135937.

References

1 Humidity Sensor Market Size, Share | Global Industry Report, 2019–2025, **https://www.grandviewresearch.com/industry-analysis/humidity-sensor-market**, (accessed June 30, 2022).
2 Humidity Sensors Market Size, Trends, Research, Industry | 2022–27, **https://www.mordorintelligence.com/industry-reports/humidity-sensors-market**, (accessed June 30, 2022).
3 M. Riede, D. Spoltore and K. Leo, *Adv. Energy Mater.*, 2021, **11**, 2002653.
4 A. Aftab and Md. I. Ahmad, *Sol. Energy*, 2021, **216**, 26–47.
5 H. F. Iqbal, Q. Ai, K. J. Thorley, H. Chen, I. McCulloch, C. Risko, J. E. Anthony and O. D. Jurchescu, *Nat. Commun.*, 2021, **12**, 2352.
6 H. Farahani, R. Wagiran and M. N. Hamidon, *Sensors*, 2014, **14**, 7881–7939.
7 Y. Park and X. Chen, *J. Mater. Chem. A*, 2020, **8**, 15227–15244.
8 M. A. Najeeb, Z. Ahmad and R. A. Shakoor, *Adv. Mater. Interfaces*, 2018, **5**, 1800969.
9 X. Rao, L. Zhao, L. Xu, Y. Wang, K. Liu, Y. Wang, G. Y. Chen, T. Liu and Y. Wang, *Sensors*, 2021, **21**, 8049.

10 B. A. Kuzubasoglu, *ACS Appl. Electron. Mater.*, 2022, **4**, 4797–4807.
11 L. Torsi, A. Dodabalapur, N. Cioffi, L. Sabbatini and P. G. Zambonin, *Sens. Actuators, B*, 2001, **77**, 7–11.
12 P. Lin and F. Yan, *Adv. Mater.*, 2012, **24**, 34–51.
13 Y. D. Park, B. Kang, H. S. Lim, K. Cho, M. S. Kang and J. H. Cho, *ACS Appl. Mater. Interfaces*, 2013, **5**, 8591–8596.
14 C. Zhang, P. Chen and W. Hu, *Chem. Soc. Rev.*, 2015, **44**, 2087–2107.
15 T. Mukhopadhyaya, J. S. Wagner, H. Fan and H. E. Katz, *ACS Appl. Mater. Interfaces*, 2020, **12**, 21974–21984.
16 A. M. Zeidell, D. S. Filston, M. Waldrip, H. F. Iqbal, H. Chen, I. McCulloch and O. D. Jurchescu, *Adv. Mater. Technol.*, 2020, **5**, 2000390.
17 C. W. Fuller, P. S. Padayatti, H. Abderrahim, L. Adamiak, N. Alagar, N. Ananthapadmanabhan, J. Baek, S. Chinni, C. Choi, K. J. Delaney, R. Dubielzig, J. Frkanec, C. Garcia, C. Gardner, D. Gebhardt, T. Geiser, Z. Gutierrez, D. A. Hall, A. P. Hodges, G. Hou, S. Jain, T. Jones, R. Lobaton, Z. Majzik, A. Marte, P. Mohan, P. Mola, P. Mudondo, J. Mullinix, T. Nguyen, F. Ollinger, S. Orr, Y. Ouyang, P. Pan, N. Park, D. Porras, K. Prabhu, C. Reese, T. Ruel, T. Sauerbrey, J. R. Sawyer, P. Sinha, J. Tu, A. G. Venkatesh, S. VijayKumar, L. Zheng, S. Jin, J. M. Tour, G. M. Church, P. W. Mola and B. Merriman, *Proc. Natl. Acad. Sci. U. S. A.*, 2022, **119**, e2112812119.
18 H. Atesci, V. Kaliginedi, J. A. C. Gil, H. Ozawa, J. M. Thijssen, P. Broekmann, M. Haga and S. J. van der Molen, *Nat. Nanotechnol.*, 2018, **13**, 117–121.
19 C. A. Nijhuis, W. F. Reus, J. R. Barber and G. M. Whitesides, *J. Phys. Chem. C*, 2012, **116**, 14139–14150.
20 X. Chen, M. Roemer, L. Yuan, W. Du, D. Thompson, E. del Barco and C. A. Nijhuis, *Nat. Nanotechnol.*, 2017, **12**, 797–803.
21 L. Cademartiri, M. M. Thuo, C. A. Nijhuis, W. F. Reus, S. Tricard, J. R. Barber, R. N. S. Sodhi, P. Brodersen, C. Kim, R. C. Chiechi and G. M. Whitesides, *J. Phys. Chem. C*, 2012, **116**, 10848–10860.
22 F. C. Simeone, H. J. Yoon, M. M. Thuo, J. R. Barber, B. Smith and G. M. Whitesides, *J. Am. Chem. Soc.*, 2013, **135**, 18131–18144.
23 J. R. Barber, H. J. Yoon, C. M. Bowers, M. M. Thuo, B. Breiten, D. M. Gooding and G. M. Whitesides, *Chem. Mater.*, 2014, **26**, 3938–3947.
24 L. Yuan, N. Nerngchamnong, L. Cao, H. Hamoudi, E. del Barco, M. Roemer, R. K. Sriramula, D. Thompson and C. A. Nijhuis, *Nat. Commun.*, 2015, **6**, 6324.
25 Z. A. Lamport, A. D. Broadnax, D. Harrison, K. J. Barth, L. Mendenhall, C. T. Hamilton, M. Guthold, T. Thonhauser, M. E. Welker and O. D. Jurchescu, *Sci. Rep.*, 2016, **6**, 38092.
26 D. Xiang, X. Wang, C. Jia, T. Lee and X. Guo, *Chem. Rev.*, 2016, **116**, 4318–4440.
27 R. M. Metzger, *Nanoscale*, 2018, **10**, 10316–10332.
28 Z. A. Lamport, A. D. Broadnax, B. Scharmann, R. W. Bradford III, A. DelaCourt, N. Meyer, H. Li, S. M. Geyer, T. Thonhauser, M. E. Welker and O. D. Jurchescu, *ACS Appl. Mater. Interfaces*, 2019, **11**, 18564–18570.
29 M. Li, B. Tu, B. Cui, X. Zhao, L. Yang, Q. Fang, Y. Yan and B. A. Grzybowski, *ACS Appl. Electron. Mater.*, 2019, **1**, 2295–2300.
30 G. D. Kong, S. E. Byeon, S. Park, H. Song, S.-Y. Kim and H. J. Yoon, *Adv. Electron. Mater.*, 2020, **6**, 1901157.
31 Y. Liu, X. Qiu, S. Soni and R. C. Chiechi, *Chem. Phys. Rev.*, 2021, **2**, 021303.
32 R. P. Sullivan, J. T. Morningstar, E. Castellanos-Trejo, R. W. Bradford III, Y. J. Hofstetter, Y. Vaynzof, M. E. Welker and O. D. Jurchescu, *Sci. Adv.*, 2022, **8**, eabq7224.
33 T. Someya, A. Dodabalapur, J. Huang, K. C. See and H. E. Katz, *Adv. Mater.*, 2010, **22**, 3799–3811.
34 L. Torsi, M. Magliulo, K. Manoli and G. Palazzo, *Chem. Soc. Rev.*, 2013, **42**, 8612–8628.
35 D. Duarte and A. Dodabalapur, *J. Appl. Phys.*, 2012, **111**, 044509.
36 B. de Boer, A. Hadipour, M. M. Mandoc, T. van Woudenbergh and P. W. M. Blom, *Adv. Mater.*, 2005, **17**, 621–625.
37 Y. Mei, D. Fogel, J. Chen, J. W. Ward, M. M. Payne, J. E. Anthony and O. D. Jurchescu, *Org. Electron.*, 2017, **50**, 100–105.
38 M. Waldrip, O. D. Jurchescu, D. J. Gundlach and E. G. Bittle, *Adv. Funct. Mater.*, 2020, **30**, 1904576.
39 J. S. Kim, B. Lägel, E. Moons, N. Johansson, I. D. Baikie, W. R. Salaneck, R. H. Friend and F. Cacialli, *Synthetic Metals*, 2000, **111**, 311–314.
40 J. W. Ward, M. A. Loth, R. J. Kline, M. Coll, C. Ocal, J. E. Anthony and O. D. Jurchescu, *J. Mater. Chem.*, 2012, **22**, 19047–19053.
41 B. de Boer, A. Hadipour, R. Foekema, T. van Woudenbergh, M. M. Mandoc, V. D. Mihailetchi and P. W. M. Blom, in *Organic Optoelectronics and Photonics*, SPIE, 2004, vol. 5464, pp. 18–25.
42 K.-Y. Wu, S.-Y. Yu and Y.-T. Tao, *Langmuir*, 2009, **25**, 6232–6238.
43 S. Watcharinyanon, E. Moons and L. S. O. Johansson, *J. Phys. Chem. C*, 2009, **113**, 1972–1979.
44 S. L. Shostak, W. L. Ebenstein and J. S. Muenter, *J. Chem. Phys.*, 1991, **94**, 5875–5882.
45 J. G. Wasserman, K. J. Murphy and J. J. Newby, *J. Phys. Chem. A*, 2019, **123**, 10406–10417.
46 S. R. Banks, J. T. Morningstar and M. E. Welker, *Molbank*, 2021, M1251.